

EDGE ARTICLE

[View Article Online](#)
[View Journal](#) | [View Issue](#)Cite this: *Chem. Sci.*, 2024, 15, 15610

All publication charges for this article have been paid for by the Royal Society of Chemistry

CO₂-actuated spin transition tuning in an interdigitated Hofmann-type coordination polymer†Abhik Paul,^a Wataru Kosaka,^{bc} Bhart Kumar,^{‡a} Dibya Jyoti Mondal,^{‡a} Hitoshi Miyasaka^{*bc} and Sanjit Konar^{‡a}

The increased anthropogenic emission level of CO₂ urges the development of CO₂-responsive materials, but is it possible to regulate the inherent electronic properties through weak physisorption of a ubiquitous gas such as CO₂? Herein, we intended to answer this imperative question by the first case of CO₂-actuated variable spin-state stabilisation in an interdigitated Hofmann-type coordination polymer [Fe^{II}Pd(CN)₄L₂] (1, L = methyl isonicotinate), showing a wide shift in transition temperature (T_{eq}) from 178 K at P_{CO_2} = 0 kPa to 229 K at P_{CO_2} = 100 kPa. Interestingly, the emergence of a stepped behaviour in the heating process below P_{CO_2} = 10 kPa and overlapping magnetic susceptibility values above P_{CO_2} = 10 kPa elucidate the selective LS state stabilisation solely correlated with the extent of CO₂ accommodation. Based on the magnetic response and phase transition diagrams obtained under respective P_{CO_2} , a plausible scenario of the spin-state switching can be interpreted as ($1_{ls} + 1'_{hs}$) → ($1_{hs} + 1'_{ls}$) → 1_{hs} at $P_{CO_2} \leq 10$ kPa, $1'_{ls} \rightarrow 1_{hs}$ at $100 \text{ kPa} < P_{CO_2} \leq 32 \text{ kPa}$ and $1'_{ls} \rightarrow 1'_{hs} \rightarrow 1_{hs}$ at 100 kPa , where 1 and 1' represent CO₂-free and CO₂-encapsulated states, respectively. The cooperative CO₂ sorption with SCO based on the varied CO₂ pressure corroborates a novel case for developing CO₂-responsive magnetic materials henceforth.

Received 28th June 2024
Accepted 28th August 2024

DOI: 10.1039/d4sc04266b

rsc.li/chemical-science

Introduction

Switchable magnetic materials that can be reversibly inter-converted between two stable states in response to an external stimulus are promising candidates for potential memory devices.^{1–5} Metal complexes, such as metal–organic frameworks (MOFs)^{6–8} or porous coordination polymers (PCPs),^{9,10} that are capable of accommodating guest molecules are of high interest in this regard as the inherent porous nature can be used to separate similar guest species^{11–13} or even exhibit guest-induced changes in their intrinsic properties,¹⁴ including emission,¹⁵ magnetic^{16,17} and conductive properties,¹⁷ amongst others.^{18–21}

Preceded by the remarkable example of guest-responsive bidirectional spin-state switching,^{22,23} the spin-crossover (SCO) research outcome investigated the influence of subtle interactions exerted by small guest molecules on effective spin-state stabilisation of PCPs.^{24–26} Nonetheless, the use of ubiquitous gas molecules (such as N₂, O₂ or CO₂) to modulate SCO behaviour in PCPs is underdeveloped,^{27–29} as the significant variation of the crystal lattice volume resulting from the change in the spin-state with relatively weak physisorption of the gas remains highly unlikely,^{30–32} compared to the chemical pressure³³ exerted by guests such as small organic molecules or solvents.^{34,35} Recent advances in the gas-responsive magnetic phase transitions revolve around utilising nanometric pores and^{36,37} open metal sites,^{38,39} the use of paramagnetic gases,⁴⁰ or even interlayer charge transfer^{41–43} by manipulating the electronic states. However, obtaining a significant SCO response only through the physisorption of a gas such as CO₂ can be narrowed down to a monomeric Co^{II} complex⁴⁴ and a 3D pseudo-Hofmann type framework.⁴⁵ While the former case demonstrates the SCO induction in the CO₂-admixed state, the latter forfeits the SCO activity. Herein, we bridge this leap in the literature by reporting the first case of fine-tuning the spin states of an interdigitated Hofmann-type PCP [Fe^{II}Pd(CN)₄L₂] (1, L = methyl isonicotinate), solely based on the selective physisorption of CO₂ molecules in the framework.

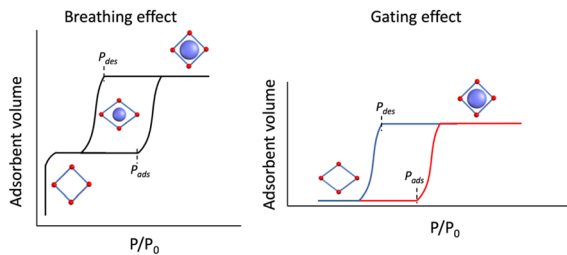
^aMolecular Magnetism Lab, Department of Chemistry, Indian Institute of Science Education and Research, Bhopal, Madhya Pradesh, India, 462066. E-mail: skonar@iiserb.ac.in

^bInstitute for Materials Research, Tohoku University, 2-1-1 Katahira, Aoba-ku, Sendai 980-8577, Japan. E-mail: miyasaka@imr.tohoku.ac.jp

^cDepartment of Chemistry, Graduate School of Science, Tohoku University, 6-3 Aramaki-Aza-Aoba, Aoba-ku, Sendai 980-8578, Japan

† Electronic supplementary information (ESI) available: Experimental and crystallographic details, additional structural views, PXRD patterns, FT-IR spectra, TGA data, and additional magnetic measurement information. CCDC 2336307. For ESI and crystallographic data in CIF or other electronic format see DOI: <https://doi.org/10.1039/d4sc04266b>

‡ These authors contributed equally.



Scheme 1 (Left) Breathing effect vs. (right) gating effect in gas adsorption of porous coordination polymers.

Traditionally, for a flexible porous crystal, the “breathing effect” is demonstrated by a drastic expansion/contraction in the pore volume upon increasing the partial pressure of the adsorbent, usually leading to a two-step gas uptake, constituted of (i) a transition from the originally opened pore to a closed pore and (ii) opening of the closed pore (Scheme 1, left). On the other hand, the abrupt increase in the adsorption capacity due to the structural change or oscillations induced by the guest admission/release is referred to as the “gating effect” (Scheme 1, right), which is much more diverse and involves intricate structural flexibility than simple expansion/contraction.^{14,46}

Compared to the typically observed classical type I adsorption isotherms (Fig. 1a), a more energetically favourable cooperative transition constitutes adsorption over a narrow pressure range and engages high working capacities defined as the amount of gas adsorbed (Fig. 1b). On a temperature scale, the consecutive temperatures of such a bistable process can be defined as T_{GO} and T_{GC} (GO, gate opening and GC, gate closing, for adsorption and desorption, respectively), and the difference

between them comprises the admixed state, based on the mode of temperature swing. Interestingly, such a “gating effect” can be correlated with the cooperative SCO dynamics where spin-state change defines the working capacity between the two states (Fig. 1c) using a thermal hysteresis loop ($\Delta T = T_{\text{heat}} - T_{\text{cool}}$).⁴⁷ However, to successfully integrate the SCO behaviour under the particular effect of physisorption, *i.e.*, without the coordination to open metal centres or any of the functional groups, the adsorbate must (i) possess a flexible and porous structural pattern to allow reversible insertion and removal of the adsorbent and (ii) the adsorbate-adsorbent interactions must be present as a subtle balance between the exerted chemical pressure in favour of the HS state and the electrostatic interactions in favour of the LS state, to regulate high cooperativity in the crystal lattice. In addition, the adsorbent must possess a necessary dipole or quadrupole moment that promotes insertion into the adsorbate framework.

Inspired by our earlier demonstration of the modulation of cooperativity from a single-to-four-step transition by de/resolution of MeOH molecules in a 2D Hofmann-type PCP **1**·1.3MeOH,⁴⁸ we sought to rationalise the system under the effect of a supercritical gas, such as CO₂, which could only impart weak dispersive interactions in the system. Notably, removal of the MeOH molecules from **1**·1.3MeOH exerts stronger π -stacking interactions between the panelling ligands, leading to our assumption that the intriguing gate-opening/closing mechanism might be achieved under the influence of CO₂. Herein, we report the first example of CO₂-actuated spin transition tuning in **1**, associated with a wide transition temperature shift from 171 K (cooling)/185 K (heating) at $P_{\text{CO}_2} = 0$ kPa to 213 K (cooling)/244 K (heating) at $P_{\text{CO}_2} = 100$ kPa with a maximum thermal hysteresis loop of ~ 65 K at $P_{\text{CO}_2} = 10$ kPa.

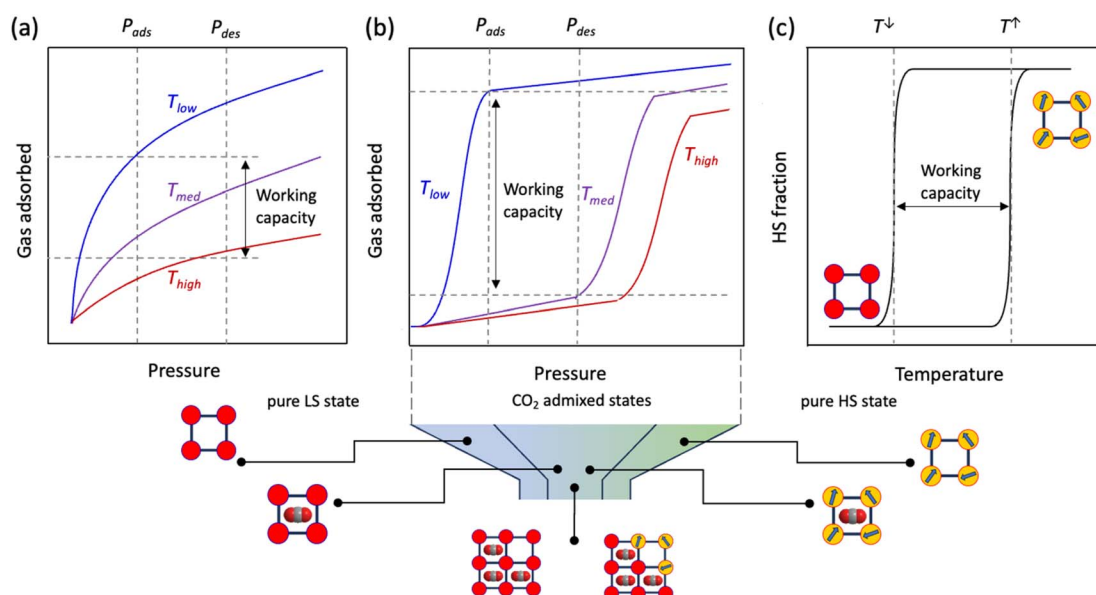


Fig. 1 Idealised adsorption isotherms and the cooperative spin-transition mechanism. (a) and (b) Comparison of the working capacities for idealised gas adsorption isotherms of (a) classical and (b) cooperative adsorbents using a smaller temperature swing, and (c) temperature-dependent hysteric spin transition. (Below) Schematic representation of the cooperative spin-transition under a CO₂ atmosphere and pure LS states at low temperature before CO₂ adsorption (**1_s**), followed by CO₂ admixed states (**1'**), based on T_{GO} and T_{ST} and pure HS states above T_{GC} . T_{GO} , T_{GC} and T_{ST} correspond to gate opening, gate closing and spin transition temperatures, respectively.



The highly selective CO₂ sorption and CO₂-responsive spin-state stabilisation can be tuned by varying the amount of CO₂ uptake, *i.e.*, P_{CO_2} .

Results and discussion

Single crystal X-ray diffraction analysis of **1**·1.3MeOH showed that each of the Fe^{II} atoms is coordinated axially by two methyl isonicotinate ligands and equatorially by the cyanide linkers of four [Pd(CN)₄]^{2−} units, forming a {Fe[Pd(CN)₄]}_∞ grid with Fe₂Pd₂ square windows. Two such grids are arranged by inter-ligand hydrogen bonding and lone pair... π interactions between the carboxylate groups and π e[−] cloud of the two adjacent pyridyl rings, resulting in an interdigitated (2D) framework (Fig. 2).

As indicated by the thermogravimetric analysis, framework **1** possesses excellent thermal stability up to 230 °C (Fig. S1, ESI†). Comparison of the PXRD spectrum of **1** with that of the parent framework **1**·1.3MeOH showed that the framework pattern in the desolvated phase is preserved (Fig. S2, ESI†), although a structural phase transition is evident from the shifting of peaks in the middle region ($2\theta = 15\text{--}25^\circ$). FTIR spectra of **1**·1.3MeOH and **1** indicate that the bonding of **1**·1.3MeOH is preserved in **1** (Fig. S3, ESI†). The variable temperature PXRD diffraction analyses of **1** showed a thermally induced-phase transition accompanied by SCO, as indicated by the peak shift near the SCO transition temperature in both cooling and heating processes (Fig. S4, ESI†). Structural flexibility deduced

for **1** to house small guest molecules such as MeOH encouraged us to check its adsorption capability for any gas molecules. However, no adsorption for N₂ (77 K) and O₂ (90 K) was observed even at 120 K (for both N₂ and O₂, Fig. S5, ESI†). In contrast, above $T \geq 195$ K, a sharp transition in the CO₂ adsorption appeared, ~ 15 kPa CO₂ pressure (P_{CO_2}), which resulted in the gate opening (GO) transition, and on increasing P_{CO_2} , reached an adsorbed amount of ~ 50 ml_{STP} g^{−1} (~ 1 molecule per formula unit) at 100 kPa (Fig. 3a). The GO pressure (for adsorption) and GC pressure (for desorption) steadily increased with the temperature increase (up to 230 K). The temperature dependence of the GO and GC pressure obeyed the Clausius–Clapeyron relationship, $d(\ln P_G)/d(\ln T_G^{-1}) = \Delta H_{\text{Trans}}/R_g$, where ΔH_{Trans} is the variation in the transition enthalpy and R_g is the universal gas constant (Fig. 3c, S6 and S7, ESI†), with estimated enthalpy values of -27 kJ mol^{−1} and -52 kJ mol^{−1} for GO and GC, respectively.⁴⁹ The gated behaviour was also characterised using the isobar plots (Fig. 3b), and for both cases, wide hysteresis was observed (Fig. S6, ESI†). Based on these data, the phase diagram of **1** under CO₂ (T vs. P_{CO_2} plot in Fig. 3c) was created for the GO and GC processes, revealing an apparent phase transition between **1** and **1**·CO₂, respectively.

Since **1** possesses a more restricted accessible pore, *i.e.*, structural reorganisation accessible only under the influence of a small guest, we expected an interplay of the SCO response with CO₂ adsorption. To check the consequence of the CO₂-gated behaviour in the respective magnetic properties of **1**, variable temperature magnetic susceptibility measurements (10–300 K) at 0.5 K min^{−1} under an external magnetic field (H_{dc}) of 1 kOe were conducted under varied CO₂ pressure using a home-built gas cell (Experimental details, ESI†). First, after loading the sample in the magnetometer, the gas cell was filled with 100 kPa He (instead of vacuum) to enhance thermal conductivity. Upon cooling, a HS-to-LS transition was observed at 171 K (171 K *in vacuo*), while a complete LS-to-HS transition was observed upon heating at 185 K (186 K *in vacuo*) revealing a bistable region of 14 K ($\Delta T = T_{\text{H}} - T_{\text{C}}$; Fig. 4a, closed circle), which perfectly reproduces the SCO behaviour (T_{eq} , ~ 178 K; $T_{\text{eq}} = (T_{\text{H}} + T_{\text{C}})/2$, where T_{eq} , T_{H} , and T_{C} refer to the average temperature of ST and transition temperature in heating and cooling mode, respectively) of the guest-free framework **1** under vacuum (Fig. 4a, open circle). Notably, the coincidence of ST phenomena in these

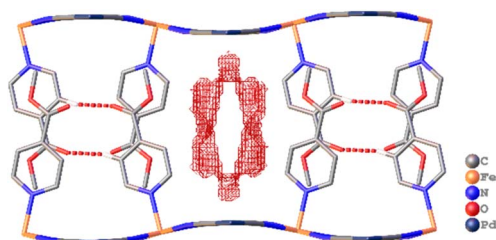


Fig. 2 Interdigitated structure of framework **1**·1.3MeOH, stabilised by inter-ligand hydrogen bonding and lone pair... π interactions, and adsorbent accessible voids are shown along crystallographic axis *a*. Solvent MeOH molecules and H atoms are omitted for visual clarity.

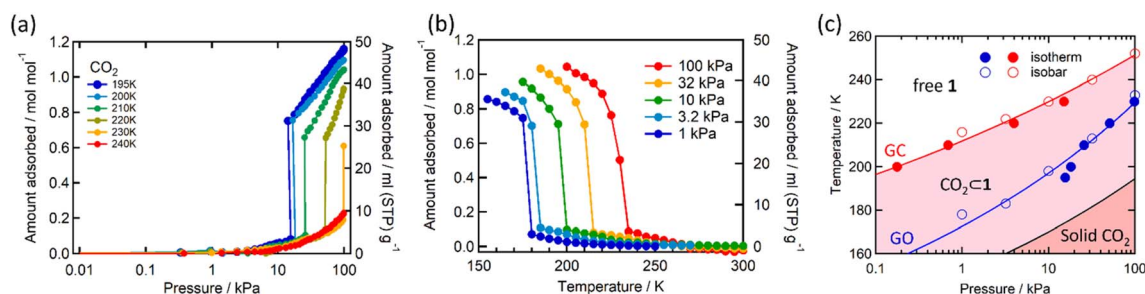


Fig. 3 CO₂ adsorption in **1** studied as (a) isotherms at different temperatures, (b) isobars at different CO₂ pressures (solid lines are a guide for the eye), and (c) phase diagram for **1**/**1'**/CO₂ determined from these measurements. The red (GC) and blue (GO) lines represent the fitting curves based on the Clausius–Clapeyron equation (ESI†). The black solid line represents the saturated vapor pressure curve, distinguishing between the solid and gas phases of bulk CO₂.



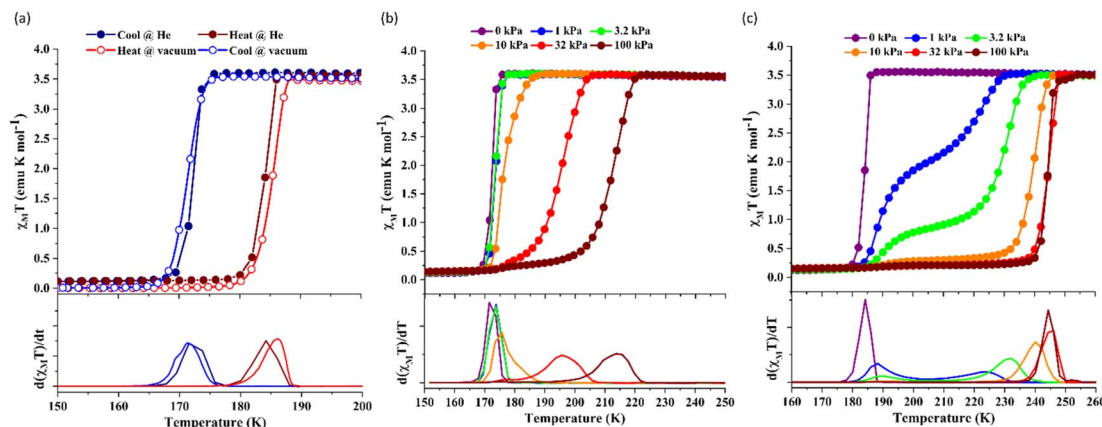


Fig. 4 Variation of the magnetic properties of framework **1** under CO_2 adsorption under $H_{\text{dc}} = 1$ kOe. (a) Magnetic susceptibility plots in the absence of any gas (open circles) and under 100 kPa He gas (filled circles). (b) The CO_2 pressure dependence of the magnetic susceptibility measurements in cooling and (c) heating mode. First derivative plots are displayed at the bottom.

two cases dismissed the possibility of any additional LS state stabilisation under the effect of applied gas pressure. Although the slight changes in the transition temperatures (T_{c} and T_{H}) and the thermal hysteresis (ΔT , 15 K *in vacuo* vs. 14 K under 100 kPa He) can be attributed to the modification in experimental setups.

Next, CO_2 gas at $P_{\text{CO}_2} = 1, 3.2, 10, 32$, and 100 kPa was introduced in the cell at 300 K, and the M - T measurements at $H_{\text{dc}} = 1$ kOe were performed consecutively in the cooling and heating mode (10–300 K). For the cooling mode shown in Fig. 4b, a one-step transition from HS-to-LS was observed with a gradual increase in the ST temperature (T_{c} ; 173 K at $P_{\text{CO}_2} = 1.0$ kPa to 213 K at $P_{\text{CO}_2} = 100$ kPa) with increased CO_2 pressure. Meanwhile, the LS-to-HS transition in the heating mode appeared in a stepwise fashion at $P_{\text{CO}_2} \leq 10$ kPa, in which $T_{\text{H}(1)}$ for the transition at lower temperature was approximately at 188 K in the all P_{CO_2} range of 1–10 kPa, while $T_{\text{H}(2)}$ for the transition at higher temperature was increased from 224 K ($P_{\text{CO}_2} = 1.0$ kPa) to 240 K ($P_{\text{CO}_2} = 10$ kPa), elucidating that the physisorption of the CO_2 molecules in the framework stabilise the LS state. Interestingly, the T_{c} and $T_{\text{H}(2)}$, defined by the peak maxima of $\delta\chi_{\text{M}}T/\delta T$ vs. T plot (Fig. 4, bottom), differ significantly under the same P_{CO_2} , indicating the presence of thermal hysteresis (ΔT) with a temperature spread up to ~ 65 K at $P_{\text{CO}_2} = 10$ kPa (Fig. 4 and Table S1, ESI†). Similarly, the observed T_{eq} variation correlates well with the result obtained from CO_2 adsorption, which indicates that the abrupt SCO behaviour observed for **1** under the CO_2 atmosphere is mainly associated with the gate-opening CO_2 adsorption process.

Apparently, the emergence of the stepped behaviour in the heating process under low CO_2 pressure ($P_{\text{CO}_2} < 10$ kPa) intrigued us to investigate the plausible scenario that occurs during the transition under the CO_2 atmosphere. The phase, as well as the spin state, for each process strongly depends on a relationship of three factors: (i) the CO_2 occupation rate in the compound, (ii) GO and GC temperatures at each CO_2 pressure applied, and (iii) intrinsic ST temperatures of pristine **1** and the CO_2 -accommodated phase **1'**. Furthermore, the nature of each

phase is basically determined by the cooling process under an applied CO_2 pressure.

As evidenced from the phase diagram, the GO process operates in the temperature range of ~ 160 to 230 K, while the GC process is valid in the temperature region of ~ 190 –250 K. Thus, based on the P_{CO_2} applied, a variation of the LS state stabilisation for the CO_2 -admixed state (**1'**) is presumed eventually in the temperature range of ~ 190 –230 K (Fig. 5, ESI†), based on the amount of CO_2 accommodated in the framework.

To delineate the magnetic transition under CO_2 sorption, the overall process can be described by a total of four states, *i.e.*, without CO_2 (**1_{ls}** and **1_{hs}**) and with CO_2 (**1'_{ls}** and **1'_{hs}**). In the cooling process at $P_{\text{CO}_2} = 1$ kPa, the ST at 173 K is owed to the intrinsic ST of pristine **1**, exhibiting a change from **1_{hs}** \rightarrow **1_{ls}**, because of the presence of CO_2 adsorption GO at 170 K, namely, the **1_{ls}** phase adsorbed CO_2 . Notably, the magnetic susceptibility changes around this temperature (Fig. 6a, green asterisk) manifest that the transition from **1_{ls}** to **1'_{ls}** might not be perfect due to the slow CO_2 adsorption kinetics, and the two states are mixed at temperatures below 170 K (**1_{hs}** \rightarrow **1_{ls}** \rightarrow **1'_{ls}** + **1_{ls}**, for $P_{\text{CO}_2} = 1$ kPa, Fig. 6a), whereas for $P_{\text{CO}_2} > 10$ kPa, the GO process occurs in the range of 200–230 K, and the gradual transition to

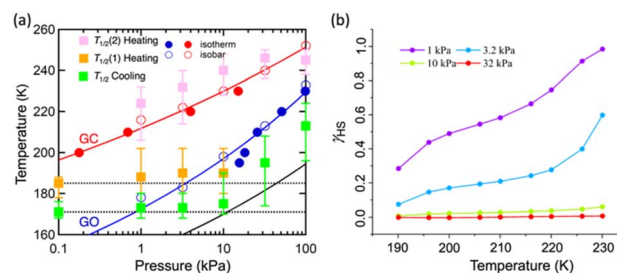


Fig. 5 (a) Correlation of the gated CO_2 sorption behaviour with the SCO transition temperatures of framework **1** under variable CO_2 pressures in the temperature range of 160–260 K; (b) HS fraction population (χ_{HS}) of **1** under variable CO_2 pressures ($P_{\text{CO}_2} = 1$ to 32 kPa) in the temperature range of 190–230 K.



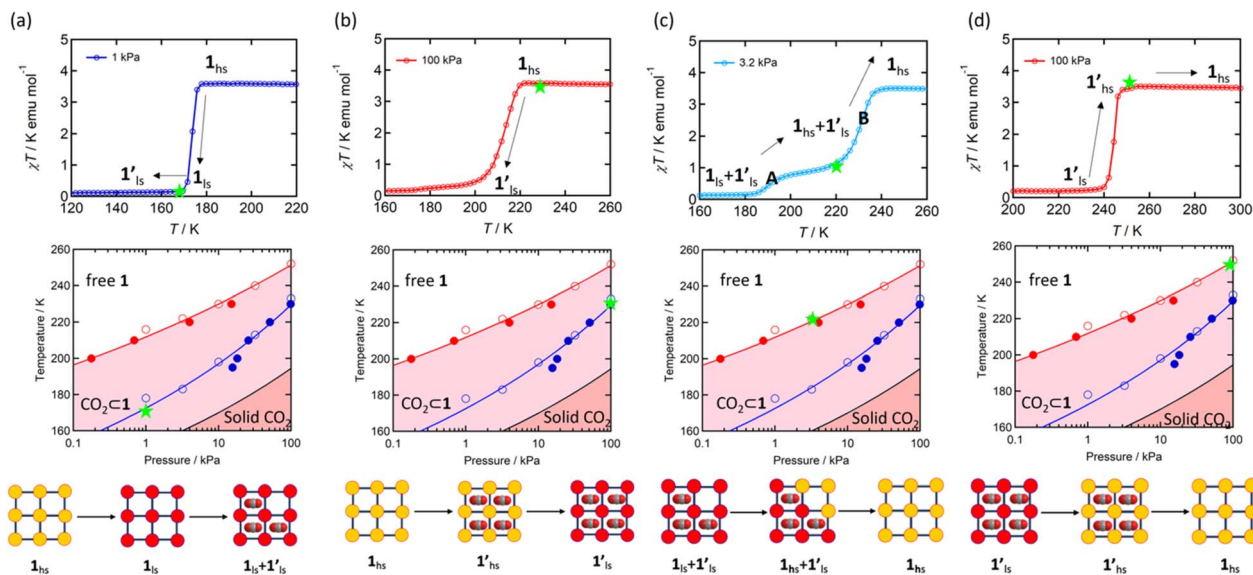


Fig. 6 (Top) Comparative magnetic transition plots under the influence of a CO₂ atmosphere in cooling ((a) 1.0 kPa; (b) 100 kPa) and heating ((c) 3.2 kPa; (d) 100 kPa) cycles; (bottom) the GO and GC temperatures denoted by green asterisk in the respective phase diagram, and a representative cartoon diagram of the SCO phenomenon occurring between different spin states of the framework 1. The red (GC) and blue (GO) lines in the phase diagram represent the fitting curves based on the Clausius–Clapeyron equation.

the diamagnetic (LS) state occurs after or with the CO₂ adsorption ($1_{\text{hs}} \rightarrow 1'_{\text{hs}} \rightarrow 1'_{\text{ls}}$, for $P_{\text{CO}_2} = 100$ kPa, Fig. 6b). Therefore, in the cooling cycle for $P_{\text{CO}_2} > 10$ kPa, the CO₂-accommodated phase prevailed because of $T_{\text{GO}} > T_{\text{C}}$; the 1_{hs} phase adsorbed CO₂, indicating $1_{\text{hs}} \rightarrow 1'_{\text{hs}}$, followed by the ST at T_{C} . However, the CO₂ occupation in the material was still dependent on the CO₂ pressure, so the phase at $P_{\text{CO}_2} = 10$ kPa can be assigned to be a mixture of ($1_{\text{hs}} + 1'_{\text{hs}}$) followed by the ST to the ($1_{\text{ls}} + 1'_{\text{ls}}$) phase at 175 K, although the ratio of $1_{\text{hs}}/1_{\text{ls}}$ (i.e., $1 \cdot \text{CO}_2$) was much lower than that of $1'_{\text{hs}}/1'_{\text{ls}}$ (Fig. 5, right). The heating process well displays the nature of the CO₂-accommodated mixture. Interestingly, at $P_{\text{CO}_2} < 10$ kPa, the gated adsorption in the framework occurs in a stepwise fashion, with an increase in temperature, leading to two distinctive forms A and B (Fig. 6c shows an instance at $P_{\text{CO}_2} = 3.2$ kPa). Below 173 K, a mixed state of $1'_{\text{ls}} + 1_{\text{ls}}$ (form A) is active, and the SCO occurs from the non-CO₂ adsorbed domain, i.e., $1_{\text{ls}} \rightarrow 1_{\text{hs}}$. The ($1'_{\text{ls}} + 1_{\text{hs}}$) mixed state B prevails in a step-level in the temperature range of 173–220 K. The second form B undergoes a CO₂ release at $T_{\text{GC}} = 220$ K, accompanied by SCO transition $1'_{\text{ls}} \rightarrow 1_{\text{hs}}$. On the other hand, the transition at $P_{\text{CO}_2} = 100$ kPa at $T_{\text{H}} = 245$ K is due to the intrinsic SCO phenomenon for $1 \cdot \text{CO}_2$, i.e., $1'_{\text{ls}} \rightarrow 1'_{\text{hs}}$, because $T_{\text{GC}} = 253$ K $>$ T_{H} (Fig. 6d), unlike the desorption-induced SCO observed at $P_{\text{CO}_2} < 10$ kPa. For $P_{\text{CO}_2} = 32$ kPa, the steep transition at ~ 240 K just overlapped with the SCO transition of $1'_{\text{ls}} \rightarrow 1'_{\text{hs}}$ and CO₂ release from $1'_{\text{ls}} \rightarrow 1_{\text{hs}}$. The materials at $P_{\text{CO}_2} < 10$ kPa are mixtures of 1 and $1 \cdot \text{CO}_2$, whose ratios were determined to be $\sim 72\%$, $\sim 85\%$ and $\sim 98\%$ $1 \cdot \text{CO}_2$ states induced at 226 K by CO₂ accommodation at $P_{\text{CO}_2} = 1$, 3.2, and 10 kPa, respectively (Table S2 and Fig. S11, ESI†). We also carried out *in situ* PXRD measurements to check the structural changes during the adsorption and SCO process (Fig. S12, ESI†);

four states (1_{ls} , 1_{hs} , $1'_{\text{ls}}$, and $1'_{\text{hs}}$) are distinguishable in PXRD patterns, providing further evidence of the SCO and gated adsorption process shown in Fig. 6.

Based on the above phenomenon of the CO₂-adsorption actuated spin transition, we were intrigued to check the generality of this method for similar guest molecules such as CS₂, which was reported to stabilise the LS states for 3D Hofmann-type framework $\{\text{Fe}(\text{pyrazine})[\text{Pt}(\text{CN})_4]\}$.^{23,50,51} Thus, $1 \cdot \text{CS}_2$ was prepared by a liquid-to-liquid slow diffusion technique using a methanolic solution of CS₂ as the buffer layer (Experimental section, ESI†). Single crystal X-ray diffraction analysis performed at 100 K showed that $1 \cdot \text{CS}_2$ crystallises in a monoclinic crystal system in space group *I2/c*, similar to the parent framework $1 \cdot 1.3\text{MeOH}$ (monoclinic *C2/c*, at 90 K). While the interdigitated nature was retained, two of the CS₂ molecules were found to lie in the middle of the Fe₂Pd₂ windows of two parallel $\{\text{Fe}[\text{Pd}(\text{CN})_4]\}_{\infty}$ grids with a short contact distance of 3.871 Å with the nearest Pd centres and an array of C–H \cdots S interactions with the surrounding ligands (Fig. S13, ESI†). However, the Fe–N equatorial (2.041 and 2.030 Å with Pd(CN)₄ units) and axial (2.117 Å with panelling ligands) bond lengths were found more towards the HS state, in stark contrast to $1 \cdot 1.3\text{MeOH}$. However, the instability of the sample at room temperature due to rapid guest loss puts a restriction on carrying out the dc magnetic susceptibility measurements of the CS₂ analogue.

This structural anomaly for the CS₂-encapsulated framework $1 \cdot \text{CS}_2$ can be attributed to the larger atomic size and low electronegativity of the S in CS₂ exerting a significant chemical pressure to result in the HS state of the Fe atoms, diminishing the cooperative communication between the metal centres. On the other hand, the relatively smaller size and high



electronegativity of O in CO₂ facilitate the electrostatic interactions within framework 1, which is a prerequisite for gated sorption behaviour and predominantly stabilises the LS state with increased absorbate pressure.

Conclusions

Although the investigation of CO₂ capture using MOFs has been quite explored lately, it is rare that they display CO₂-induced changes in their structure and properties.⁵² The present study provides an efficient and straightforward strategy for the magnetic phase changes *in situ* by tuning the physisorption amount of CO₂ without any change in the chemical properties of framework 1. Based on the magnetic response and the phase transition diagram obtained under the respective *P*_{CO₂}, the key factor of the overall spin-state switching can be interpreted as the stabilisation of LS states under the influence of CO₂. We are hopeful that the insights gathered from this work into understanding the mechanism by which switchable properties can be controlled by gas adsorption will be helpful for the development of future CO₂-responsive materials for practical applications.

Data availability

Experimental and crystallographic details, additional structural views, PXRD patterns, FT-IR spectra, TGA data, and additional magnetic measurement information are provided in the ESI.†

Author contributions

All authors have given approval to the final version of the manuscript. AP and SK conceptualised the project; BK and DJM prepared and performed physical characterisation of the frameworks; WK performed the adsorption studies and magnetic measurements under CO₂; AP and WK interpreted the data and the working concept; AP, SK, and HM prepared the manuscript.

Conflicts of interest

There are no conflicts to declare.

Acknowledgements

This work was supported by the Science and Engineering Research Board (SERB), India, under the project Core Research Grant (Project No. CRG/2022/001676), IISER Bhopal, a Grant-in-Aid for Scientific Research (no. 20H00381, 21H01900, and 21K18925) from MEXT, Japan, and the GIMRT and the E-IMR projects at the Institute for Materials Research, Tohoku University. AP, DJM and BK thank the Council of Scientific and Industrial Research (CSIR), India, for providing Senior Research Fellowships. SK acknowledges IISER Bhopal for instrumental support.

Notes and references

- 1 A. Paul, A. Gupta and S. Konar, *Cryst. Growth Des.*, 2021, **21**, 5473–5489.
- 2 A. Paul and S. Konar, *J. Mater. Chem. C*, 2022, **10**, 4980–4984.
- 3 Y. Cui, B. Li, H. He, W. Zhou, B. Chen and G. Qian, *Acc. Chem. Res.*, 2016, **49**, 483–493.
- 4 A. Paul, R. Nasani, A. Mondal, S. Roy, S. Vela and S. Konar, *Cryst. Growth Des.*, 2020, **20**, 6296–6301.
- 5 O. Sato, *Nat. Chem.*, 2016, **8**, 644–656.
- 6 H. Furukawa, K. E. Cordova, M. O'Keeffe and O. M. Yaghi, *Science*, 2013, **341**, 1230444.
- 7 A. Kirchon, L. Feng, H. F. Drake, E. A. Joseph and H.-C. Zhou, *Chem. Soc. Rev.*, 2018, **47**, 8611–8638.
- 8 O. I.-F. Chen, C.-H. Liu, K. Wang, E. Borrego-Marin, H. Li, A. H. Alawadhi, J. A. R. Navarro and O. M. Yaghi, *J. Am. Chem. Soc.*, 2024, **146**, 2835–2844.
- 9 E. Coronado and G. Mínguez Espallargas, *Chem. Soc. Rev.*, 2013, **42**, 1525–1539.
- 10 G. Mínguez Espallargas and E. Coronado, *Chem. Soc. Rev.*, 2018, **47**, 533–557.
- 11 S. Li, W. Han, Q.-F. An, K.-T. Yong and M.-J. Yin, *Adv. Funct. Mater.*, 2023, 2303447.
- 12 S.-M. Wang, M. Shivanna, S.-T. Zheng, T. Pham, K. A. Forrest, Q.-Y. Yang, Q. Guan, B. Space, S. Kitagawa and M. J. Zaworotko, *J. Am. Chem. Soc.*, 2024, **146**, 4153–4161.
- 13 M. Shivanna, K.-i. Otake, S. Hiraide, T. Fujikawa, P. Wang, Y. Gu, H. Ashitani, S. Kawaguchi, Y. Kubota, M. T. Miyahara and S. Kitagawa, *Angew. Chem., Int. Ed.*, 2023, **62**, e202308438.
- 14 A. Schneemann, V. Bon, I. Schwedler, I. Senkovska, S. Kaskel and R. A. Fischer, *Chem. Soc. Rev.*, 2014, **43**, 6062–6096.
- 15 Z. Hu, B. J. Deibert and J. Li, *Chem. Soc. Rev.*, 2014, **43**, 5815–5840.
- 16 J. Zhang, W. Kosaka, K. Sugimoto and H. Miyasaka, *J. Am. Chem. Soc.*, 2018, **140**, 5644–5652.
- 17 J. Zhang, W. Kosaka, Y. Kitagawa and H. Miyasaka, *Angew. Chem., Int. Ed.*, 2019, **58**, 7351–7356.
- 18 Q. Wang and D. Astruc, *Chem. Rev.*, 2020, **120**, 1438–1511.
- 19 S. Parshamoni, R. Nasani, A. Paul and S. Konar, *Inorg. Chem. Front.*, 2021, **8**, 693–699.
- 20 S. Khatua, S. Goswami, S. Biswas, K. Tomar, H. S. Jena and S. Konar, *Chem. Mater.*, 2015, **27**, 5349–5360.
- 21 A. Paul, S. D. Adhikary, S. Kapurwan and S. Konar, *J. Mater. Chem. A*, 2022, **10**, 13152–13169.
- 22 G. J. Halder, C. J. Kepert, B. Moubaraki, K. S. Murray and J. D. Cashion, *Science*, 2002, **298**, 1762–1765.
- 23 M. Ohba, K. Yoneda, G. Agustí, M. C. Muñoz, A. B. Gaspar, J. A. Real, M. Yamasaki, H. Ando, Y. Nakao, S. Sakaki and S. Kitagawa, *Angew. Chem., Int. Ed.*, 2009, **48**, 4767–4771.
- 24 B. Kumar, A. Paul, D. J. Mondal, P. Paliwal and S. Konar, *Chem. Rec.*, 2022, **22**, e202200135.
- 25 M. Feng, Z.-Y. Ruan, Y.-C. Chen and M.-L. Tong, *Chem. Commun.*, 2020, **56**, 13702–13718.
- 26 S.-G. Wu, L.-F. Wang, Z.-Y. Ruan, S.-N. Du, S. Gómez-Coca, Z.-P. Ni, E. Ruiz, X.-M. Chen and M.-L. Tong, *J. Am. Chem. Soc.*, 2022, **144**, 14888–14896.



- 27 P. D. Southon, L. Liu, E. A. Fellows, D. J. Price, G. J. Halder, K. W. Chapman, B. Moubaraki, K. S. Murray, J.-F. Létard and C. J. Kepert, *J. Am. Chem. Soc.*, 2009, **131**, 10998–11009.
- 28 J. W. Shin, A. R. Jeong, S. Jeoung, H. R. Moon, Y. Komatsumaru, S. Hayami, D. Moon and K. S. Min, *Chem. Commun.*, 2018, **54**, 4262–4265.
- 29 E. Coronado, M. Gimenez-Marques, G. Minguez Espallargas, F. Rey and I. J. Vitorica-Yrezabal, *J. Am. Chem. Soc.*, 2013, **135**, 15986–15989.
- 30 C. Serre, F. Millange, C. Thouvenot, M. Noguès, G. Marsolier, D. Louër and G. Férey, *J. Am. Chem. Soc.*, 2002, **124**, 13519–13526.
- 31 C. Mellot-Draznieks, C. Serre, S. Surblé, N. Audebrand and G. Férey, *J. Am. Chem. Soc.*, 2005, **127**, 16273–16278.
- 32 S. Horike, S. Shimomura and S. Kitagawa, *Nat. Chem.*, 2009, **1**, 695–704.
- 33 K. Lin, Q. Li, R. Yu, J. Chen, J. P. Attfield and X. Xing, *Chem. Soc. Rev.*, 2022, **51**, 5351–5364.
- 34 D. J. Mondal, B. Kumar, A. Paul and S. Konar, *J. Mater. Chem. C*, 2023, **11**, 6750–6759.
- 35 R. Turo-Cortés, C. Bartual-Murgui, J. Castells-Gil, M. C. Muñoz, C. Martí-Gastaldo and J. A. Real, *Chem. Sci.*, 2020, **11**, 11224–11234.
- 36 W. Kosaka, H. Nemoto, K. Nagano, S. Kawaguchi, K. Sugimoto and H. Miyasaka, *Chem. Sci.*, 2023, **14**, 791–800.
- 37 W. Kosaka, Y. Hiwatashi, N. Amamizu, Y. Kitagawa, J. Zhang and H. Miyasaka, *Angew. Chem., Int. Ed.*, 2023, **62**, e202312205.
- 38 E. Coronado, M. Giménez-Marqués, G. M. Espallargas and L. Brammer, *Nat. Commun.*, 2012, **3**, 828.
- 39 E. D. Bloch, W. L. Queen, R. Krishna, J. M. Zadrozny, C. M. Brown and J. R. Long, *Science*, 2012, **335**, 1606–1610.
- 40 W. Kosaka, Z. Liu, J. Zhang, Y. Sato, A. Hori, R. Matsuda, S. Kitagawa and H. Miyasaka, *Nat. Commun.*, 2018, **9**, 5420.
- 41 J. Zhang, W. Kosaka, Y. Kitagawa and H. Miyasaka, *Nat. Chem.*, 2021, **13**, 191–199.
- 42 J. Zhang, W. Kosaka, H. Sato and H. Miyasaka, *J. Am. Chem. Soc.*, 2021, **143**, 7021–7031.
- 43 J. Zhang, W. Kosaka, Q. Liu, N. Amamizu, Y. Kitagawa and H. Miyasaka, *J. Am. Chem. Soc.*, 2023, **145**, 26179–26189.
- 44 M. Nakaya, W. Kosaka, H. Miyasaka, Y. Komatsumaru, S. Kawaguchi, K. Sugimoto, Y. Zhang, M. Nakamura, L. F. Lindoy and S. Hayami, *Angew. Chem., Int. Ed.*, 2020, **59**, 10658–10665.
- 45 M. Magott, K. Płonka, B. Sieklucka, K. Dziedzic-Kocurek, W. Kosaka, H. Miyasaka and D. Pinkowicz, *Chem. Sci.*, 2023, **14**, 9651–9663.
- 46 C. R. Murdock, B. C. Hughes, Z. Lu and D. M. Jenkins, *Coord. Chem. Rev.*, 2014, **258**, 119–136.
- 47 S. Brooker, *Chem. Soc. Rev.*, 2015, **44**, 2880–2892.
- 48 D. J. Mondal, A. Mondal, A. Paul and S. Konar, *Inorg. Chem.*, 2022, **61**, 4572–4580.
- 49 K. Uemura, S. Kitagawa, K. Fukui and K. Saito, *J. Am. Chem. Soc.*, 2004, **126**, 3817–3828.
- 50 K. Scanda, Y. Avila, R. Mojica, R. Amaro, B. Portales-Martínez, M. González, M. Avila, B. D. Moreno and E. Reguera, *Colloids Surf., A*, 2023, **676**, 132114.
- 51 H. Ando, Y. Nakao, H. Sato, M. Ohba, S. Kitagawa and S. Sakaki, *Chem. Phys. Lett.*, 2011, **511**, 399–404.
- 52 N. Yanai, K. Kitayama, Y. Hijikata, H. Sato, R. Matsuda, Y. Kubota, M. Takata, M. Mizuno, T. Uemura and S. Kitagawa, *Nat. Mater.*, 2011, **10**, 787–793.

